Powder magnetoresistance of $Tl_2Mn_2O_7$ and related compounds

2004 J. Phys.: Condens. Matter 16 3465

(http://iopscience.iop.org/0953-8984/16/20/017)

INSTITUTE OF PHYSICS PUBLISHING JOURNAL OF PHYSICS: CONDENSED MATTER

J. Phys.: Condens. Matter **16** (2004) 3465–3480 PII: S0953-8984(04)72847-7

Powder magnetoresistance of $Tl_2Mn_2O_7$ and related compounds

M Venkatesan[1], P Velasco[1,2], J A Alonso[2], J L Martínez[2] and J M D Coey[1]

[1] Physics Department, Trinity College Dublin, Dublin 2, Republic of Ireland
[2] Instituto de Ciencia de Materiales de Madrid, CSIC, Cantoblanco, E-28049 Madrid, Spain

Received 3 December 2003
Published 7 May 2004
Online at stacks.iop.org/JPhysCM/16/3465
DOI: 10.1088/0953-8984/16/20/017

Abstract

The magnetoresistance of pressed powder compacts of the manganese pyrochlore $Tl_2Mn_2O_7$, including samples diluted with Al_2O_3 powder and the substituted materials $(Tl_{1.8}Bi_{0.2})Mn_2O_7$ and $Tl_2(Mn_{1.8}Te_{0.2})O_7$, is compared with that of dense ceramic samples of the same materials. The resistivity of the pressed powders, which is several orders of magnitude greater than that of the ceramics, usually shows a negative magnetoresistance which varies as H^2 both above and below the Curie point T_C; the quadratic variation is observed in the ceramics only above T_C. The H^2 variation below T_C, which is unlike that found in other half-metallic oxides, is associated with the semimetallic character of $Tl_2Mn_2O_7$ which leads to the presence of misaligned spins at the surfaces of the powder particles. When $Tl_2Mn_2O_7$ powder is mixed with different volume fractions of Al_2O_3, the magnetoresistance near the percolation threshold at 54% $Tl_2Mn_2O_7$ is found to be dominated by a few tunnel barriers, and there is evidence for Coulomb blockade in both the I:V and R:T curves.

1. Introduction

The pyrochlore manganite $Tl_2Mn_2O_7$ is a cubic compound with an interesting electronic structure and unexpected magnetic properties [1, 2]. The crystal structure is illustrated in figure 1. There are eight formula units per unit cell. The Mn^{4+} ions are octahedrally coordinated by oxygen, and they form a corner-sharing tetrahedral array, which is similar to that of the B-sites in the spinel structure. In a simple ionic picture, the material would be an insulator containing $Mn^{4+}(3d^3)$ and $Tl^{3+}(5d^{10})$ cations. Only the former bear a magnetic moment of 3 μ_B due to a $t_{2g}^{3\uparrow}$ configuration and they couple via 133° Mn–O–Mn superexchange bonds. Antiferromagnetic Mn^{4+}–O–Mn^{4+} superexchange is highly frustrated by the three-membered rings of the tetrahedral array. The pyrochlore manganites $Sc_2Mn_2O_7$ and $Y_2Mn_2O_7$ are insulators with low magnetic ordering temperatures (∼20 K) and random spin freezing [3, 4], similar to that in $ZnFe_2O_4$.

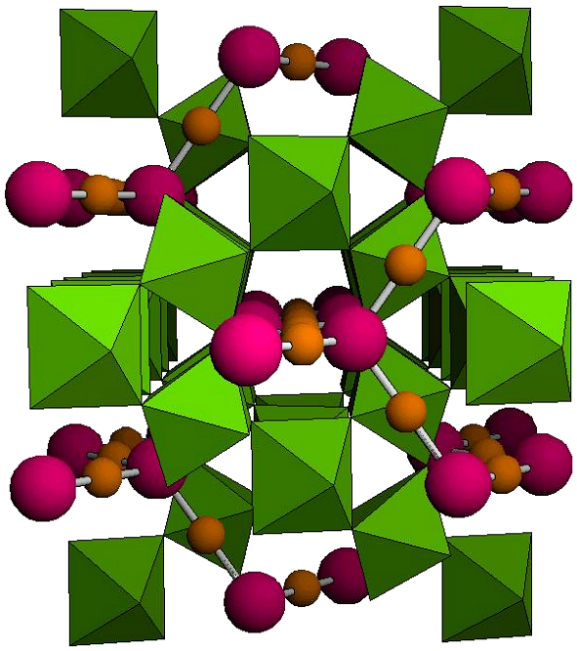

Figure 1. Crystal structure of $Tl_2Mn_2O_7$ showing the tetrahedral manganese array.

The thallium compound, however, is a ferromagnetic semimetal with a small number of heavy holes at the top of a narrow ↑ band of mainly $Mn(t_{2g})$ character and an equal number of mobile ↓ electrons in a broad band of mixed Tl(6s), O(2p) and Mn(3d) character [4–6], as indicated in figure 2. The number of carriers has been estimated at 0.086 per unit cell [5] or 0.005 per manganese from LSDA-LAPW calculations. Other calculations [4, 6] give 0.04 or 0.24 carriers per unit cell, but all agree on the semimetallic structure. The mobile ↓ electrons are expected to dominate the conduction, while the heavy ↑ holes, for which the Fermi energy lies just 0.07 eV below the top of the band, will be easily localized by any impurities or disorder that may be present in the compound. $Tl_2Mn_2O_7$ can also be regarded as a half-metal insofar as the ↑ holes do not contribute significantly to the conduction; it has been classified as a type IVb or $G_{\alpha'\beta}$ half-metal [7]. Measurements of the Hall effect confirm the electronic structure predictions to the extent that the Hall coefficient is negative, and corresponds, in a one-band model, to 0.01–0.05 electrons per unit cell [1, 8].

The ↓ carriers in $Tl_2Mn_2O_7$ mediate the ferromagnetic coupling. The situation is different in the perovskite manganites such as $(La_{0.7}Ca_{0.3})MnO_3$ where the transport of $Mn(e_g^{\uparrow})$ carriers propagates the double exchange interaction. Here, as in ferromagnetic double perovskites such as Sr_2FeMoO_6 [9], a separate ↓ electronic system is involved which hybridizes with the 3d core orbitals of the Mn or Fe to provide the coupling. The Mn–O–Mn superexchange is a weaker interaction on account of the 133° bond angle [6, 10].

The pure $Tl_2Mn_2O_7$ pyrochlore exhibits a positive temperature coefficient of resistance below the Curie temperature $T_C \approx 118$ K. Its rather high resistivity is consistent with metallic conduction for a low carrier density. There is a one or two order of magnitude increase in ρ near T_C, where a 'colossal' negative magnetoresistance is observed in a high magnetic field [1, 2]. The value of T_C, the magnitude of resistivity peak near T_C for $Tl_2Mn_2O_7$, and the corresponding magnetoresistance are greatly altered by isovalent (Sc, Bi, Ru) or aliovalent (Cd, Sb, Te) substitution [11–16].

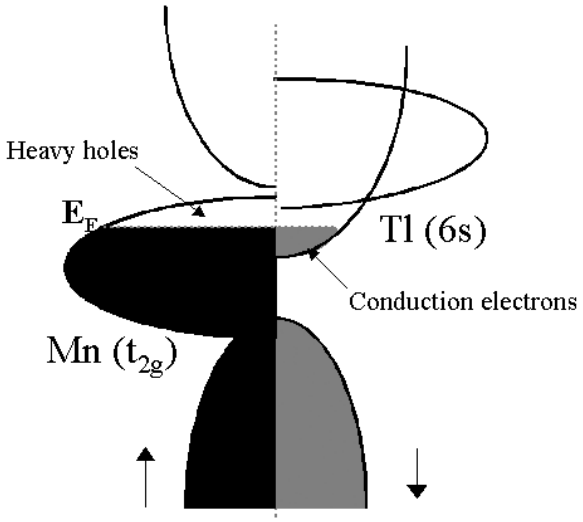

Figure 2. Schematic electronic structure of $Tl_2Mn_2O_7$ [5]. It is a semimetal, with localized ↑ holes and mobile ↓ electrons (a type IVb half-metal [7]). At the surface the bands are narrower, and they do not overlap.

Since the pyrochlores are produced by high-pressure synthesis, all transport data have been collected on dense ceramic samples. Grain boundaries are well-known to play an important part in determining the resistivity and magnetoresistance of metallic oxides [17–20]. Notably, a low-field contribution to the magnetoresistance in the ferromagnetic state which is almost linear in field, varying as $|H|$, is attributed to the alignment of the magnetization of adjacent grains, separated by a grain boundary [17]. Hysteresis is often seen, giving rise to a characteristic 'butterfly' magnetization curve.

In the vicinity of T_C, the intrinsic colossal magnetoresistance effect may become very pronounced, especially in suitably doped material [12, 14]. Above T_C, the magnetoresistance $\Delta\rho/\rho(0)$ varies as $c(M/M_s)^2$, where M is the magnetization induced by the applied field, M_s is the saturation magnetization and $\Delta\rho = \rho(0) - \rho(H)$; in low fields, the magnetoresistance, defined as $\Delta\rho/\rho(0)$, varies as H^2. The coefficient $c = 15$ reported for $Tl_2Mn_2O_7$ [1] is larger than for most other materials, including the mixed-valence manganites. The large value has been attributed to intrinsic spin-disorder scattering, where the coefficient c scales as $n^{-2/3}$, n being the electron density [21, 22]. More generally [20], a resistance varying as

$$\rho = \rho(0)\exp[-c(M/M_s)^2] \tag{1}$$

offers a phenomenological description of the behaviour of a wide range of ferromagnetic oxides near and above T_C. This expression reduces to $\Delta\rho/\rho(0) = c(M/M_s)^2$ when $(M/M_s) \leqslant 0.2$.

Large negative 'butterfly' magnetoresistance effects have been reported for pressed powders of various ferromagnetic materials including the half-metallic oxides CrO_2, Fe_3O_4, $(La_{0.7}Sr_{0.3})MnO_3$ and Sr_2FeMoO_6 [23–26]. By physically separating the crystallites and pressing them together in a powder compact, electrical contact is achieved with minimum exchange coupling between the adjacent grains [26]. Besides offering a quick method of estimating the degree of spin polarization, powder magnetoresistance allows us to focus on the interparticle transport that dominates the resistance of the compacts. Here we apply the method to ferromagnetic $Tl_2Mn_2O_7$ and related pyrochlores in an effort to understand the origin of the magnetoresistance in these materials.

Table 1. Physical properties of pure, and Bi- and Te-doped $Tl_2Mn_2O_7$ samples.

	Pure	Bi	Te
a_0 (Å)	9.9001	9.9233	9.9226
V (m^3)	9.70×10^{-28}	9.77×10^{-28}	9.78×10^{-28}
ρ_x (kg m^{-3})	8634	8586	8773
d_{ceramic} (nm)	500 ± 300	600 ± 170	200 ± 80
$\rho_{\text{ceramic}}/\rho_x$	0.79	0.81	0.80
d_{powder} (nm)	330 ± 30	670 ± 90	240 ± 30
$\rho_{\text{powder}}/\rho_x$	0.48	0.41	0.38
ρ (200 K) (Ω m)	0.163	17.31	1.14×10^{-3}
ρ (4 K) (Ω m)	8.33×10^{-4}	138.6	8.38×10^{-4}
R_c (MΩ)	0.324	2.39	0.005
T_c (K)	118	81	190
M_s (5 K) (μ_B/fu)	4.18	3.80	4.19
M_s (kA m^{-1})	318	289	319
$\mu_0 M_s$ (T)	0.40	0.36	0.40
n (e^- m^{-3}) (Hall)	9.8×10^{23}	—	1.34×10^{26}
f(O′)	0.960(6)	0.942(6)	0.98(1)
f(Tl)	0.972(3)	0.892(2)	0.945(6)
f(M)	—	0.091(2)	0.054(5)

2. Experimental methods

The compounds studied here are: $Tl_2Mn_2O_7$, $Tl_2(Mn_{1.8}Te_{0.2})O_7$ and $(Tl_{1.8}Bi_{0.2})Mn_2O_7$. All the pyrochlores were prepared from the oxides by high-pressure synthesis (2 GPa) in sealed gold tubes at 1300 K, as described elsewhere [12]. The phase purity of the compounds was checked using powder x-ray diffraction. A standard four-probe method was used to measure the resistivity and magnetoresistance in the range 4–300 K using a commercial 5 or 9 T SQUID magnetometer or a 1.2 T MULTIMAG set-up. The MULTIMAG is a permanent-magnet variable flux source which provides a transverse field in the bore which can be varied both in magnitude and direction. Resistivity measurements were performed on dense ceramic samples using the four-probe method. For powder magnetoresistance (PMR) measurements, the ceramics were ground using a mortar and pestle to a grain size of about 0.3 μm, which corresponds roughly to the crystallite size. The powder was then compressed at 12 MPa into a disc about 0.8 mm thick and 5 mm in diameter. In one series of measurements, the $Tl_2Mn_2O_7$ powder was diluted with various amounts of insulating α-Al_2O_3 powder of approximately the same grain size. Densities of the ceramics were measured by weighing in CCl_4 and those of the pressed powder compacts were deduced from the mass of the cylindrical pellets.

3. Results

All compounds exhibit a single-phase cubic pyrochlore structure with no sign of any secondary phase. The refined lattice parameters are included in table 1. Electron micrographs of the ceramics and powder compacts of the pure end-member, and the Bi- and Te-doped material are shown in figure 3. The densities and grain sizes are listed in table 1; typical relative densities of ceramics and powders are about 80% and 50%, respectively. The temperature dependence of the resistivity of ceramic, powder and composites with Al_2O_3 are shown in figure 4. The powder compact and the ceramic have resistivities that differ only by a factor of ten above T_C, but the gap between them widens to two orders of magnitude below 100 K.

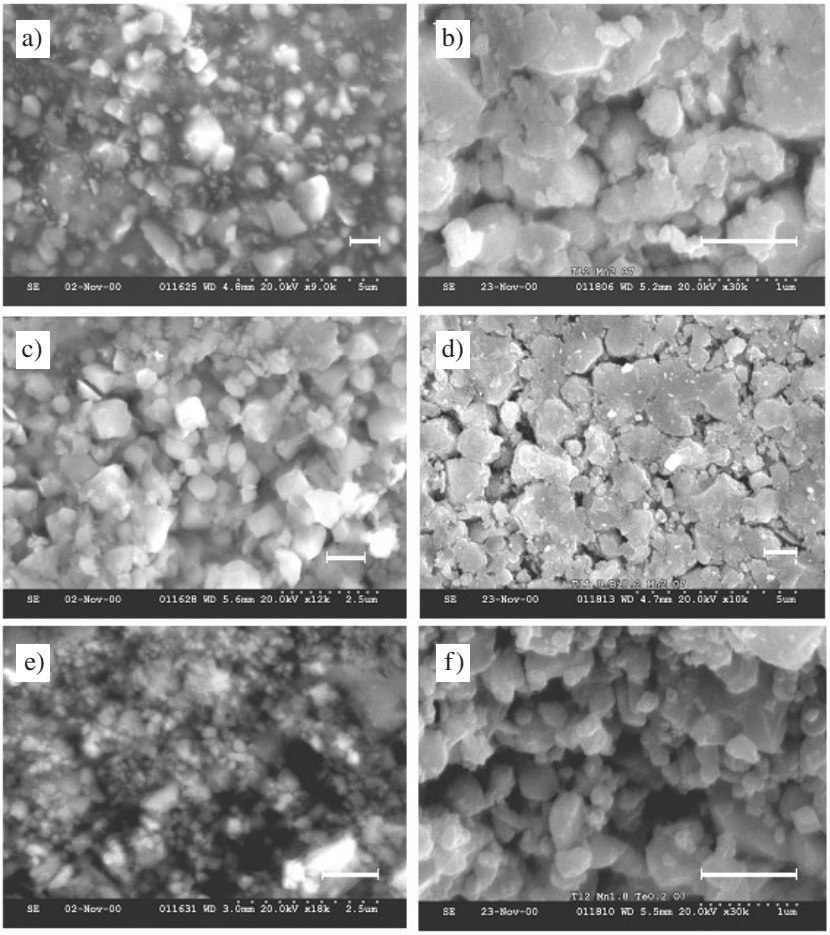

Figure 3. Electron micrographs of (a) $Tl_2Mn_2O_7$ ceramic, (b) $Tl_2Mn_2O_7$ powder, (c) $(Tl_{1.8}Bi_{0.2})Mn_2O_7$ ceramic, (d) $(Tl_{1.8}Bi_{0.2})Mn_2O_7$ powder, (e) $Tl_2(Mn_{1.8}Te_{0.2})O_7$ ceramic and (f) $Tl_2(Mn_{1.8}Te_{0.2})O_7$ powder. The scale bars represent 1 μm.

The greater resistivity of the powder compact is attributed to the resistance of the interparticle contacts. One can expect a very broad distribution of contact resistance, which will direct the conduction along percolation paths encompassing the lower resistance contacts. The powder compact of $Tl_2Mn_2O_7$ shows a resistivity of 1 Ω m at room temperature, and the grain size d is about 0.3 μm. The *average* interparticle contact resistance $\langle R_c \rangle \approx \rho/d$ is therefore about 3 MΩ. The temperature dependence of the resistivity of pressed powder compacts 60% $Tl_2Mn_2O_7$:40% α-Al_2O_3 and 55% $Tl_2Mn_2O_7$:45% α-Al_2O_3 is also included in figure 4. Diluting $Tl_2Mn_2O_7$ with 40% and 45% insulating α-Al_2O_3 increases the resistivity by a further three to six orders of magnitude and produces an upturn in resistivity at low temperature typical of a dielectric granular metal [27]. Extrapolating the room-temperature conductivity of a series of compositions to zero using the percolation relation [28] $1/\rho = (x - x_c)^2$ yields the threshold concentration $x_c = 54\%$.

The I:V characteristics of the samples are generally Ohmic, with the exception of the 55% $Tl_2Mn_2O_7$:45% α-Al_2O_3 sample. The I:V curves shown in figure 5 are non-linear at 2 and 5 K, a behaviour typical of a Coulomb gap (Coulomb blockade) [29]. Furthermore,

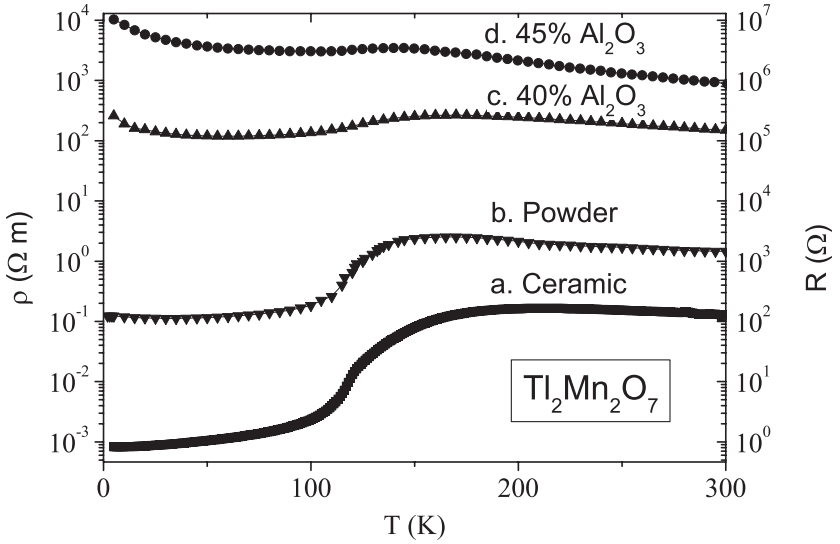

Figure 4. Temperature dependence of the resistivity of powder and ceramic samples of $Tl_2Mn_2O_7$ (a) ceramic, (b) pressed powder, (c) pressed powder 60% $Tl_2Mn_2O_7$:40% α-Al_2O_3 and (d) pressed powder 55% $Tl_2Mn_2O_7$:45% α-Al_2O_3.

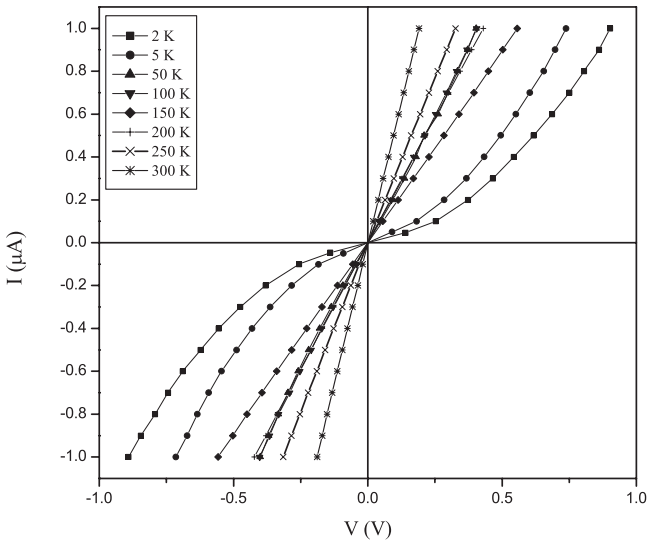

Figure 5. I:V curve for 55% $Tl_2Mn_2O_7$:45% α-Al_2O_3 pressed powder at different temperatures.

the low-temperature upturn of the resistivity in these powders is fitted by the equation $\rho = \rho_\infty \exp(\Delta/k_B T)^{1/2}$ where ρ_∞ is the resistivity at 100 K and Δ is approximately equal to the charging energy $E_C = e^2/2C$, where C is the capacitance of the ferromagnetic grains [27]. The capacitance of a small spherical metallic particle is $C = 4\pi\varepsilon_0\varepsilon_r r$ where ε_0 is the permittivity of free space, ε_r is the relative permittivity and r is the radius. If we take an average value for $r = 165$ nm and $\varepsilon_r = 5$, then C is 9.2×10^{-17} F and $E_C/k_B = 10.1$ K. Fitting the data of figure 4(d) gives $\Delta/k_B = 25$ K.

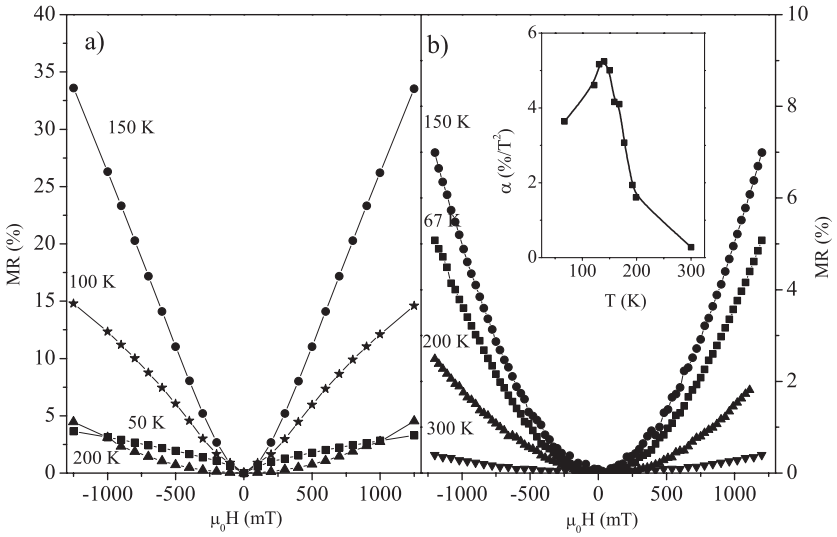

Figure 6. Magnetoresistance of (a) ceramic and (b) pressed powder samples of $Tl_2Mn_2O_7$ at different temperatures. The inset in (b) shows the temperature dependence of the H^2 term.

Turning now to the magnetoresistance, the field dependence for ceramic and pressed power compacts are shown in figure 6. Two types of behaviour may be distinguished. One is a convex H^2 dependence and the other is a concave variation beginning as $|H|$, which approaches saturation in higher fields. The ceramic sample of $Tl_2Mn_2O_7$ exhibits an H^2 variation above T_C and a $|H|$ variation below T_C, as seen in figure 6(a). Near T_C, where the magnetoresistance is most pronounced, reaching a maximum of 30% in 1 T, there is mixed behaviour. Note that although resistance *decreases* with field, the magnetoresistance plotted in figures 6 and 7 is defined to be positive.

On the other hand, the pressed powder exhibits an H^2 variation at *all* temperatures, both above below and above T_C. The temperature-dependence of the coefficient α, where $\Delta\rho/\rho_0 = \alpha\mu_0^2H^2$, is shown by the inset in figure 6(b); it reaches a maximum value around T_C where the magnetoresistance in 1 T is 5%. The value is around 0.3% in 1 T at 300 K. Figure 7 compares the powder magnetoresistance of undiluted $Tl_2Mn_2O_7$, 60% $Tl_2Mn_2O_7$:40% α-Al_2O_3 and 55% $Tl_2Mn_2O_7$:45% α-Al_2O_3 compacts at different temperatures. The magnetoresistance follows the $\alpha\mu_0^2H^2$ behaviour and is little changed at 40 vol% Al_2O_3, but at 45 vol% there is a sharp increase of resistance and a changeover from H^2 to $|H|$ behaviour at 100 K, just below T_C.

Figure 8 shows the resistivity of $Tl_2(Mn_{1.8}Te_{0.2})O_7$ and $(Tl_{1.8}Bi_{0.2})Mn_2O_7$, both ceramic and powders, as a function of temperature. The resistivity of the Te-doped powder exhibits an increase of three orders of magnitude in resistivity compared to the ceramic, but in neither case is there much of a peak at T_C (190 K). The Te-doped material shows an initially linear magnetoresistance behaviour below T_C in both ceramic and pressed powder compacts (figure 9). In the Bi-doped sample, the resistivity is two or three orders of magnitude greater than in the pure compound, and it diverges as $T \to 0$. In contrast to the Te-doped samples, the resistivity of Bi-doped ceramic and powder samples exhibits a maximum above $T_C = 81$ K, similar to undoped materials, followed by an upturn at low temperature. Magnetoresistance at 200 K of $(Tl_{1.8}Bi_{0.2})Mn_2O_7$ ceramic and powders varies as H^2, but at 50 K the powder shows an H^2 variation whereas the ceramic is a $|H|$ case (figure 9).

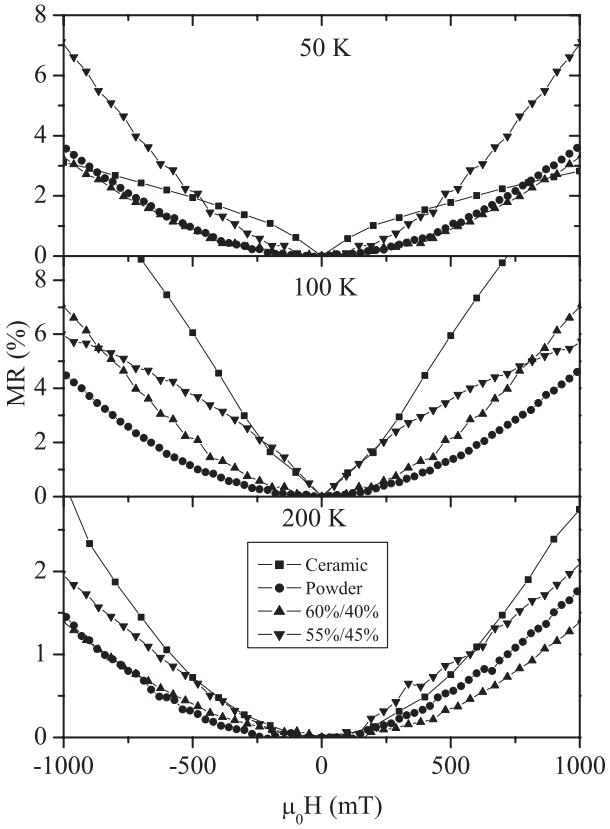

Figure 7. Comparison of powder magnetoresistance in ceramic, powder, 60% $Tl_2Mn_2O_7$:40% α-Al_2O_3 and 55% $Tl_2Mn_2O_7$:45% α-Al_2O_3 powder compacts.

4. Discussion

In order to analyse the data, we have to distinguish the intrinsic resistance and magnetoresistance of $Tl_2Mn_2O_7$ in the paramagnetic and ferromagnetic states from the contribution of the interparticle contacts. Normally, the intrinsic properties of metallic oxides can be measured directly on single crystals or epitaxial films, but in the present case these are unavailable. The best available material seems to be that of Shimakawa *et al* [1] (table 2) who find a residual resistivity $\rho_0 = 4 \times 10^{-6}$ Ω m with no marked field dependence up to 7 T for a sample fired twice at high pressure. This is one or two orders of magnitude less than ρ_0 found for other samples [11, 13], including our own. Using the expression for the mean free path $\lambda = mv_F/ne^2\rho_0$, and the values $n = 8.9 \times 10^{25}$ m^{-3}, $v_F = 3.3 \times 10^5$ m s^{-1} given by Singh [5] for the free-electron like $\downarrow$ band, a reasonable value, $\lambda = 33$ nm, is obtained. Wherever necessary, we will use theoretical values from Singh's calculation throughout the discussion; they are compared with others in table 3.

It is expected that there will be intrinsic positive terms in the magnetoresistance of a semimetal at low temperature which vary as B^2 or as $|B|$ [30]. The classical B^2 term and the quantum linear magnetoresistance are never observed for $Tl_2Mn_2O_7$, which indicates that the magnetoresistance is dominated by intergranular transport processes, or intrinsic processes of magnetic origin.

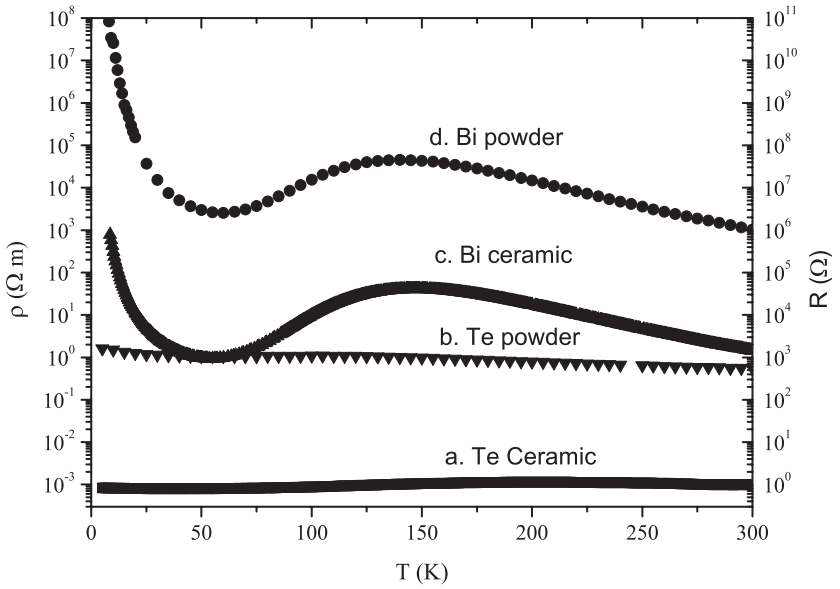

Figure 8. Temperature dependence of resistivity of (a) $Tl_2(Mn_{1.8}Te_{0.2})O_7$ ceramic, (b) $Tl_2(Mn_{1.8}Te_{0.2})O_7$ powder, (c) $(Tl_{1.8}Bi_{0.2})Mn_2O_7$ ceramic and (d) $(Tl_{1.8}Bi_{0.2})Mn_2O_7$ powder.

Table 2. Electrical properties of $Tl_2Mn_2O_7$ ceramics.

ρ_0 (Ω m)	$\rho_{300\ K}$ (Ω m)	$d\rho_{300\ K}/dT$ (Ω m K^{-1})	Reference
4×10^{-6}	3×10^{-4}	>0	Shimakawa *et al* [1]
8×10^{-5}	1×10^{-3}	>0	Ramirez and Subramanian [11]
2×10^{-5}	3×10^{-3}	<0	Hwang [34]
	1×10^{-3}	>0	Imai *et al* [8]
9×10^{-4}	1×10^{-2}	>0	Martínez *et al* [13]
2×10^{-5}	3×10^{-3}	<0	Alonso *et al* [12]
8×10^{-4}	1×10^{-1}	<0	This work

Table 3. Calculated properties of $Tl_2Mn_2O_7$.

Reference	n (m^{-3})	n (fu^{-1})	N (E_F)(↓) (eV^{-1})	v_F(↓) (m s^{-1})	k_F(↓) (m^{-1})
Singh [5]	8.9×10^{25}	0.011	0.24	3.3×10^5	2.9×10^9
Mishra and Sathpaty [6]	24×10^{25}	0.03	0.69	2.8×10^5 [a]	2.4×10^9 [a]
Shimakawa *et al* [4]	4×10^{25}	0.005	0.45	1.5×10^5 [a]	1.3×10^9 [a]

[a] Deduced from a free-electron model.

An unusual feature of $Tl_2Mn_2O_7$ is evident when the spin polarization P is evaluated using data in [5]. There are several possible definitions, P_0, P_1,P_2, where [29]

$$P_n = (N^{\uparrow} v_F^{\uparrow n} - N^{\downarrow} v_F^{\downarrow n})/(N^{\uparrow} v_F^{\uparrow n} + N^{\downarrow} v_F^{\downarrow n}) \qquad \text{for } n = 0, 1, 2. \tag{2}$$

All are equal to 100% for type I or type II half-metals where $N^{\uparrow}$ or $N^{\downarrow} = 0$. However, for type III and type IV half-metals, where both light and heavy ↑ or ↓ carriers are present at E_F, the values of P_n are quite different. For $Tl_2Mn_2O_7$, $P_0 = 66\%$, $P_1 = -5\%$ and $P_2 = -71\%$. Generally P_1 applies for ballistic transport and P_2 applies for diffusive transport

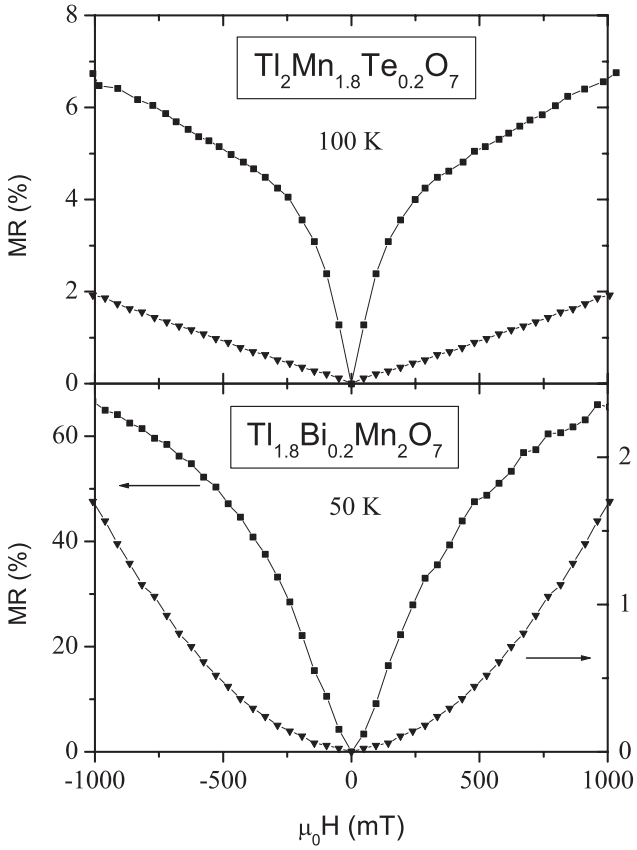

Figure 9. Magnetoresistance of $Tl_2(Mn_{1.8}Te_{0.2})O_7$ and $(Tl_{1.8}Bi_{0.2})Mn_2O_7$ below T_C. (■) Ceramic and (▼) pressed powder.

and tunnelling through a specular barrier with low transparency [31]. For undoped $Tl_2Mn_2O_7$ we therefore anticipate that very little magnetoresistance will be associated with ballistic intergranular transport.

4.1. Ceramic samples

The residual resistivity of our ceramic sample $\rho_0 = 8 \times 10^{-4}$ Ω m, together with the carrier density determined from Hall effect measurements on the same sample [32], 1.2×10^{-4} carriers per formula unit ($n = 9.8 \times 10^{23}$ m^{-3}) yields a mean free path, $\lambda = 1.5$ nm. Taking $k_F = (3\pi^2 n)^{1/3} \approx 3 \times 10^8$ m^{-1} from the free electron model, the Ioffe–Regel criterion for metallic conduction [33] $k_F\lambda > 1$ requires λ to be greater than 3.2 nm. The low temperature resistivity is therefore extrinsic. The small negative linear, low-field magnetoresistance at low temperature (figure 6(a)) which approaches saturation in a field of 1 T is attributed to intergranular tunnelling [34].

Any process where electrons tunnel or hop directly from one ferromagnetic grain to another without passing through a domain wall can give rise to a magnetoresistance varying initially as $|H|$, and saturating in fields $\mu_0 H \approx 1$ T. The reason is that each grain is subject to a stray field fM_s created by the others, where $f < 1$. Provided the exchange coupling does not propagate

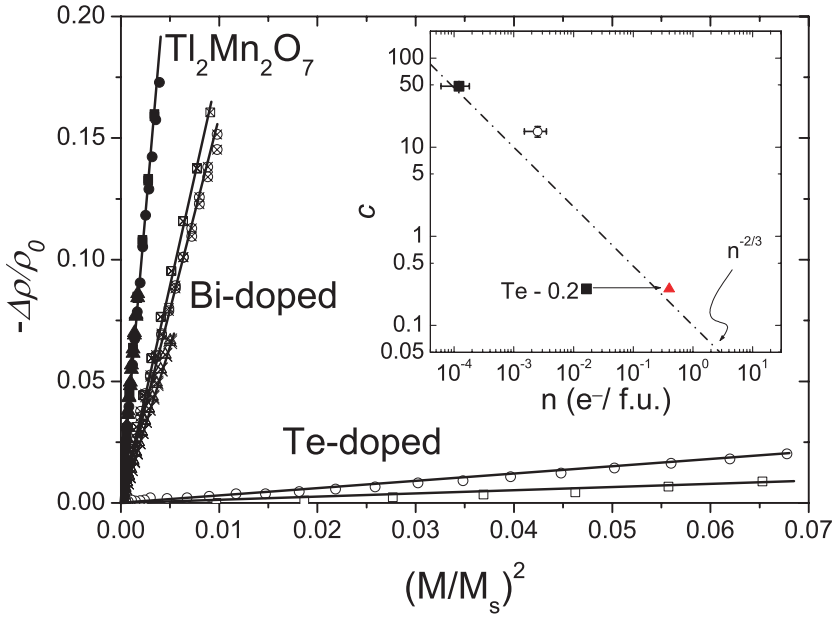

Figure 10. Variation of the magnetoresistance above T_C with $(M/M_s)^2$ for the three samples. Squares correspond to 200 K, circles to 250 K and triangles to 300 K. The coefficient c is plotted in the inset for the pure $Tl_2Mn_2O_7$ and $Tl_2(Mn_{1.8}Te_{0.2})O_7$ (■), using carrier concentrations deduced from Hall measurements. Also included is the point for $Tl_2(Mn_{1.8}Te_{0.2})O_7$ with the nominal electron concentration (▲), and the point from [1] (○).

across the grain boundary, the change in angle θ_{ij} between the direction of magnetization of two grains varies as $\delta\theta_{ij} \approx H/fM_s$ in small fields. Since the electron transfer probability depends on $\cos^2(\theta_{ij}/2) = 1/2(1+\cos\theta_{ij})$, and $\cos(\theta+\delta\theta) \approx \cos\theta - \sin\theta \times \delta\theta$, the magnetoresistance is therefore initially linear in H. It will saturate in fields $\geqslant fM_s$, where $\mu_0 M_s = 0.40$ T (table 1).

Turning to the behaviour of the $Tl_2Mn_2O_7$ ceramic above T_C, where $\rho \approx 10^{-1}$ Ω m, $n \approx 10^{22}$ m^{-3} from Hall effect, $\Delta\rho/\rho \approx H^2$, it is evident that the Ioffe–Regel criterion cannot be satisfied and that intergranular contacts are important. The question is whether the colossal magnetoresistance near T_C and the H^2 variation above T_C reflect the properties of the bulk or of the resistive intergranular regions. The magnetoresistance varies as $(M/M_s)^2$ with $c \approx 48$ (figure 10), again indicating a lower carrier density than for the Shimakawa sample [1] where $c = 15$.

Despite the high resistance, it is possible that the temperature and field-dependence do reflect intrinsic behaviour, typified by the Shimakawa sample which shows both colossal magnetoresistance and an H^2 magnetoresistance at higher temperature. How this can come about is shown schematically in figure 11. A well-sintered material (figure 11(a)) with low grain-boundary resistance exhibits intrinsic properties, including the magnitude of ρ. However, if some intergranular contacts are either missing or nonmetallic, a percolation path can still pass entirely through low resistance contacts (figure 11(b)). The maximum resistance R_{max} of such a path may be of the order of $\rho l/d^2$ where l is the sample dimension (5 mm) and d is the grain size (0.3 μm). Again using Shimakawa's data to provide an upper limit for ρ at room temperature (3×10^{-4} Ω m) gives $R_{max} = 2 \times 10^7$ Ω. However, such a thread-like percolation path is highly improbable in three dimensions where a better estimate of R_{max} would be the

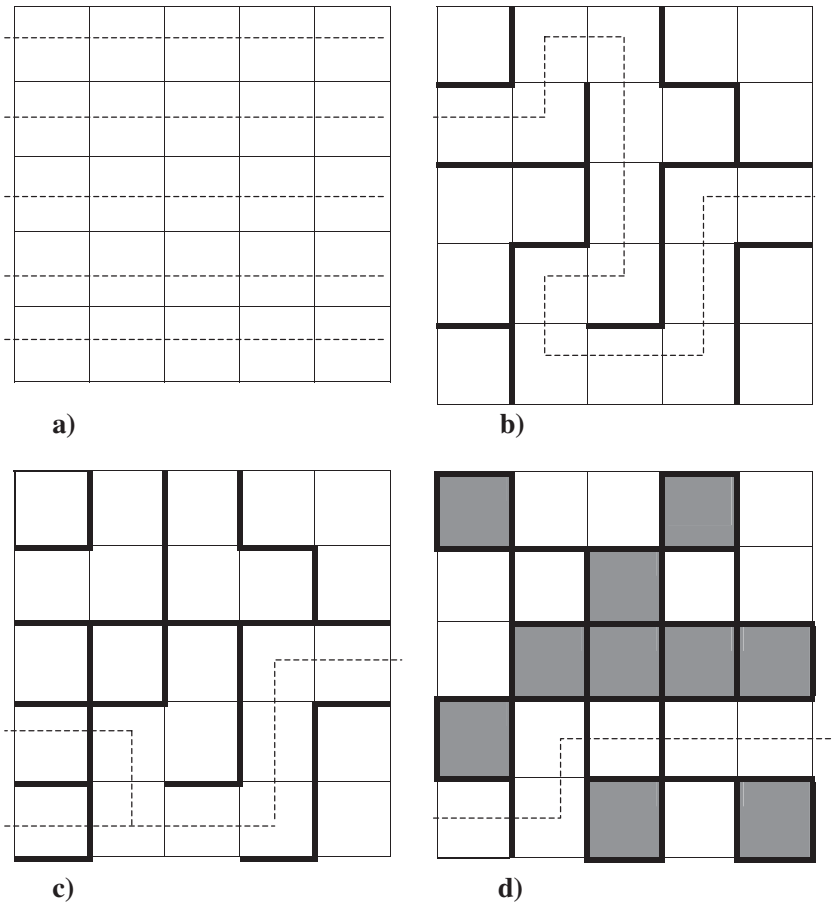

Figure 11. Schematic conduction paths through (a) a well-sintered ceramic with low-resistance grain boundaries (light lines), (b) a poorly sintered ceramic or powder compact with few or (c) many high-resistance contacts and (d) a dilute powder compact with an isolated grain in the critical path.

resistance of a single grain acting as a bottleneck; $R_{\max} = \rho/d = 10^3\ \Omega$. In any case, the point to be emphasized is that a ceramic or powder sample can exhibit a resistivity that is orders of magnitude greater than the intrinsic value, with a field and temperature dependence which are nonetheless intrinsic. Focusing on the sign of $\mathrm{d}\rho/\mathrm{d}T$ as an indication of metallic conduction, it can be seen from table 2 that samples with resistivity up to $10^{-2}\ \Omega$ m can still have a positive sign of $\mathrm{d}\rho/\mathrm{d}T$ at room temperature.

4.2. Powder samples

The extended H^2 magnetoresistance of the powder samples below T_C is absent in the dense ceramic, and must therefore be a feature of the interparticle contacts. Furthermore it has not been observed in the ferromagnetic state of any other half-metallic oxide [26]. With the exception of the 45/55 sample just below T_C, it is also evident in the dilute samples which have a high resistance ($\approx 10^7\ \Omega$) and behave like dielectric granular metals [24, 27]. The effect is not found in the highly conducting Te-doped material.

The magnetoresistance of any heterogeneous polycrystalline material is dominated by its weakest links, which could be single tunnel barriers, or one or more isolated particles, as shown in figures 11(c) and (d). The broad distribution of interparticle contact resistance may be log-normal or bimodal with maxima above and below the quantum of resistance $R_Q = h/2e^2 = 12.9\ k\Omega$, which is the maximum resistance value a metallic contact can have. The conducting path can be imagined by first joining the particles with the lowest contact resistance to form clusters, and then growing the clusters by adding progressively higher-resistance contacts until a percolation path appears between the electrodes. Continuing this process further adds paths in parallel with much higher resistance, having little influence on the net resistivity. The resistance of a sample will be of the order of the resistance of the most resistive link in the least resistive path. This will be a metallic contact when $R < R_Q$ (i.e. for the ceramic and pressed powder of the pure and Te-doped materials, where $R < 10^4\ \Omega$) but a tunnel barrier in the diluted samples where $R > R_Q$ (i.e. the diluted powders of pure and bismuth-doped material, where $R > 10^4\ \Omega$). When there is an isolated particle in the conduction path, Coulomb blockade occurs. The charging energy E_C/e for our particles is about 1 mV. The upturn in the $I{:}V$ curves above 300 mV (figure 5) indicates that there are a few hundred isolated particles among the $\approx 10^4$ in a typical conduction path.

How then does the H^2 magnetoresistance arise? Above T_C, it is related, via equation (1), to the polarization of the paramagnetic bulk material; below T_C, it is related to the polarization of the magnetically disordered interface region. Following Evetts *et al* [20], we postulate the presence of an interfacial region with magnetization M_{ip} through which the electrons have to pass when travelling from one particle to the next. This region is subject to stray fields from adjacent particles as well as the applied field, so $\mathbf{M}_{ip} = \chi_{ip}(\mathbf{H} + \Sigma_i \mathbf{H}_i)$ where $\mathbf{H}_i$ is the stray field from the ith adjacent particle; generally $\mathbf{H}_i \propto f_i \mathbf{M}_i$. The resistance varies as equation (1), and the magnetoresistance is then

$$[R(0) - R(H)]/R(0) \approx c\chi_{ip}^2(H^2 + 2\mathbf{H} \cdot \Sigma_i \mathbf{H}_i). \tag{3}$$

The second term will average to zero when the directions of $\mathbf{H}$ and $\Sigma_i \mathbf{H}_i$ are uncorrelated.

The microscopic mechanism behind the phenomenology is a matter for speculation. One possibility is spin-disorder scattering by paramagnetic atoms at the interface. Majumdar and Littlewood [21, 22] considered paramagnetic scattering of a low-density electron gas. Their model accounts for the variation of c with $n^{-2/3}$ or k_F^{-2} shown in the inset to figure 10 but a difficulty is that the corresponding condition $k_F\xi \gg 1$, is not satisfied for the bulk $Tl_2Mn_2O_7$ where the ferromagnetic correlation length ξ is of the order of the Mn–Mn separation, 0.35 nm, since $k_F \approx 0.3\text{–}3 \times 10^8\ m^{-1}$. The model suggests a thick fluctuation shell ($\sim$1 nm thick) at the particle surface.

The unusual magnetoresistance of the $Tl_2Mn_2O_7$ powder is best attributed to its semimetallic character. Band narrowing at the surface of the particles due to the reduced coordination number may make the surface semiconducting, transferring the $\downarrow$ Tl(6s) electrons over to fill the $\uparrow$ $Mn(t_{2g})$ band. The carriers would then be magnetic polarons. By removing the electrons which mediate the ferromagnetic exchange interaction, the surface spins may become paramagnetic, or adopt a non-collinear alignment under the influence of the underlying antiferromagnetic Mn–O–Mn superexchange. These surface spins can be polarized in a large applied field, as shown in figure 12. The moment that requires high field to saturate is about 1% of the total (figure 12, right inset), which corresponds to a surface shell of thickness 1 nm on a particle of radius 300 nm. The $1/H^2$ approach to saturation results from random fluctuations of a local exchange or anisotropy field. The high field itself can help to empty the $\uparrow$ $Mn(t_{2g})$ band by increasing the spin splitting, but the effect on the magnetization is one order of magnitude smaller than that due to alignment of the surface spins, which produces the

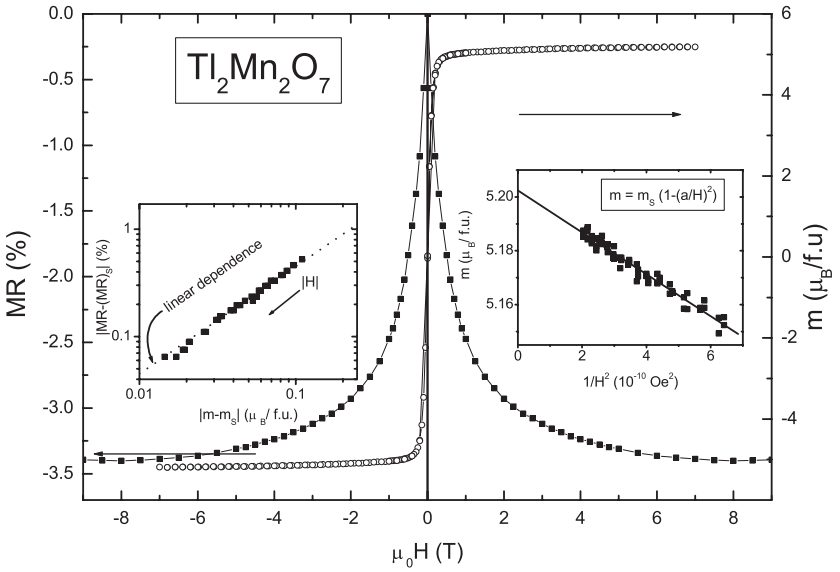

Figure 12. High-field magnetization and magnetoresistance of $Tl_2Mn_2O_7$ at 5 K. The insets show the approach to saturation of the magnetization varying as $1/H^2$, and the behaviour of the magnetoresistance mimicking that of the magnetization.

$1/H^2$ approach to saturation illustrated in the inset to figure 12. The approach to saturation of the magnetoresistance mimics that of the magnetization.

4.3. The percolation threshold

The percolation threshold lies at a volume fraction $x_p = 54\%$ in the $Tl_2Mn_2O_7/Al_2O_3$ mixture. Given that the powder compacts are only about 48% dense (table 1), this corresponds to 26% of space filled by $Tl_2Mn_2O_7$. Normally for fully-dense random media, percolation occurs at about 16%. A rule of thumb for site percolation is $x_p \approx 2/Z$, where Z is the coordination number [35]. The structure of the powder compacts is a random packing of roughly spherical particles, although the observed density is lower than for random dense packing (63%), and the rigid nature of the contacts precludes a full complement of 12–13 of them from being conducting. Using the rule of thumb, the average number of conducting contacts per particle in the undiluted compact is $2/x_p = 3.7$. The three-dimensional crystal lattice which best models this is diamond, which has four contacts.

4.4. Substituted samples

The Te-doped ceramic is metallic at all temperatures, ($\rho \approx 10^{-3}\ \Omega$ m) with a small resistivity peak near T_C, and no colossal magnetoresistance effect. $\Delta\rho/\rho$ is about 2% in 1 T at 200 K, and the value of c well above T_C is only 0.3. It is surprising that Te can substitute for Mn in this structure, but it does seem to act as Te^{6+}, a donor contributing two electrons to the conduction band, so the electron concentration is greatly increased, to about 0.4/fu or $n = 3 \times 10^{27}$ m^{-3}. Hall data, interpreted on a one-band model, give $n = 1.3 \times 10^{26}$, but there may be canceling contributions from holes and electrons and an influence of non-stoichiometry. In any case, the coefficient c, which scales as $n^{-2/3}$ [21, 22] is much reduced compared to pure $Tl_2Mn_2O_7$ (figure 10). The H^2 magnetoresistance above T_C is likewise very small in the powder

compact. However, a linear low-field effect clearly seen in both the ceramic and the powder below T_C, is associated with interparticle hopping or tunnelling (figure 9). Band narrowing does not result in a surface depleted of conduction electrons here because of the large carrier concentration.

The Bi material is localized at low temperature with indications of spin glass behaviour and it exhibits a large colossal magnetoresistance. Analysis of the low temperature upturn in resistivity shows that it fits a granular metal-type behaviour $\rho = \rho_\infty \exp(\Delta/T)^{1/2}$ rather than a semiconductor law $\rho = \rho_\infty \exp(\Delta/T)$. The value of Δ is 34 K, similar to that of the dilute $Tl_2Mn_2O_7$ samples, suggesting that the grain boundaries in the bismuth ceramic are already depleted of electrons. However, the upturn is field dependent, with the resistivity at 10 K decreasing by almost three orders of magnitude in 7 T, as the value of Δ falls from 34 to 15 K. The field-dependence is much too large to be explained in terms of the $\cos^2 \theta_{ij}/2$ dependence of the transmission probability of an electron between adjacent misoriented grains. The intrinsic semiconductor gap (if there was one) would be expected to widen rather than narrow in an applied field. The field dependence of Δ has been reported in granular metals [36], in CrO_2 powder compacts [24] and in discontinuous $La_{0.7}Ca_{0.3}MnO_3$ films [37], where it is associated with the greater population of accessible grains for hopping as the moments are aligned.

5. Conclusions

(i) The resistivity of our ceramic and pressed-powder samples of $Tl_2Mn_2O_7$ is largely determined by interparticle contacts. Nevertheless it is possible for the field and temperature dependence to reflect the intrinsic, bulk behaviour when the resistance of a sample is no more than about two orders of magnitude greater than the intrinsic resistance.

(ii) Positive intrinsic magnetoresistance terms are not observed. They are overcome by negative terms of magnetic origin.

(iii) In more resistive samples, the magnetoresistance is that of the interparticle contacts. Each particle has approximately four contacts with its neighbours.

(iv) An H^2 magnetoresistance is associated with the contacts in pressed powders of $Tl_2Mn_2O_7$, both above and below T_C. The latter behaviour has not been reported previously in a powder compact made of half-metallic material. It is attributed to the semimetallic nature of $Tl_2Mn_2O_7$, which leads to an electron-depleted, semiconducting surface layer with the full Mn^{4+} spin moment. The quadratic variation is explained phenomenologically in terms of the magnetization M_{ip} of a misaligned region at the particle surface with electron hopping or tunnelling through the interface region.

(v) When diluted with nonconducting particles near the percolation threshold, there is evidence of Coulomb blockade of particles along the percolation path. Similar behaviour is seen in the Bi-doped ceramic material, where the grain boundaries are electron-depleted.

Acknowledgments

This work was supported by Enterprise Ireland under contract SC99-225, by the EU Growth programme as part of the AMORE project and by Science Foundation Ireland. PV acknowledges a grant from the Spanish MEC.

References

[1] Shimakawa Y, Kubo Y and Manako T 1996 *Nature* **379** 53
[2] Subramanian M A, Toby B H, Ramirez A P, Marshall W J, Sleight A W and Kwei G H 1996 *Science* **273** 81
[3] Greedan J E, Raju N P and Subramanian M A 1996 *Solid State Commun.* **99** 399
[4] Shimakawa Y, Kubo Y, Hamada N, Jorgensen J D, Hu Z, Short S, Nohara M and Takagi H 1999 *Phys. Rev.* B **59** 1249
[5] Singh D J 1997 *Phys. Rev.* B **55** 313
[6] Mishra S K and Sathpaty S 1998 *Phys. Rev.* B **58** 7585
[7] Coey J M D and Venkatesan M 2002 *J. Appl. Phys.* **91** 8345
Coey J M D and Sanvito S 2004 *J. Phys. D: Appl. Phys.* **37** 988
[8] Imai H, Shimakawa Y, Sushko Yu V and Kubo Y 2000 *Phys. Rev.* B **62** 12190
[9] Kobayashi K-I, Kimura T, Sawada H, Terakura K and Tokura Y 1998 *Nature* **395** 677
[10] Nunez Regueiro M D and Lacroix C 2001 *Phys. Rev.* B **63** 014417
[11] Ramirez A P and Subramanian M A 1997 *Science* **277** 546
[12] Alonso J A, Martínez J L, Martínez-Lope M J and Casais M T 1999 *Phys. Rev. Lett.* **82** 189
[13] Martinez B, Senis R, Foncuberta J, Obradors X, Cheikh-Rouhou W, Strobel P, Bougerol-Chaillout C and Pernet M 1999 *Phys. Rev. Lett.* **83** 2022
[14] Alonso J A, Velasco P, Martínez-Lope M J, Casais M T, Martínez J L, Fernández-Díaz M T and de Paoli J M 2000 *Appl. Phys. Lett.* **76** 3274
[15] Alonso J A, Martínez-Lope M J, Casais M T, Velasco P, Martínez J L, Fernández-Díaz M T and de Paoli J M 1999 *Phys. Rev.* B **60** R15024
[16] Velasco P, Alonso J A, Martínez-Lope M J, Casais M T, Martínez J L, Fernández-Díaz M T and de Paoli J M 2001 *Phys. Rev.* B **64** 184436
[17] Huang H Y, Cheong S W, Ong N P and Batlogg B 1996 *Phys. Rev. Lett.* **77** 2041
[18] Gupta A, Gong G Q, Xiao G, Duncombe P R, Lecoeur P, Trouilloud P, Wang Y Y, Dravid V P and Sun J Z 1996 *Phys. Rev.* B **54** R15629
[19] Ziese M 2002 *Rep. Prog. Phys.* **65** 143
[20] Evetts J E, Blamire M G, Mathur N D, Isaac S P, Teo B-S, Cohen L F and MacManus-Driscoll J L 1998 *Phil. Trans. R. Soc.* A **156** 1593
[21] Majumdar P and Littlewood P 1998 *Phys. Rev. Lett.* **81** 1314
[22] Majumdar P and Littlewood P 1998 *Nature* **395** 479
[23] Borges R P, Thomas R M, Cullinan C, Coey J M D, Suryanarayanan R, Ben-Dor L, Pinsard-Gaudart L and Revcolevschi A 1999 *J. Phys.: Condens. Matter* **11** L445
[24] Coey J M D, Berkowitz A E, Balcells L1, Putris F F and Barry A 1998 *Phys. Rev. Lett.* **80** 3815
[25] Coey J M D, Berkowitz A E, Balcells L1, Putris F F and Parker F T 1998 *Appl. Phys. Lett.* **72** 734
[26] Coey J M D 1999 *J. Appl. Phys.* **85** 5576
[27] Sheng P 1992 *Phil. Mag.* B **65** 357
[28] Stauffer K 1985 *Introduction to Percolation Theory* (London: Taylor and Francis)
[29] Geerligs B 1990 Classical and quantum charge dynamics in small tunnel junctions *PhD Thesis*
[30] Abrikosov A 2003 *J. Phys. A: Math. Gen.* **36** 9119
[31] Mazin I 1999 *Phys. Rev. Lett.* **83** 1427
[32] Velasco P 2001 *PhD Thesis* Universidad Autónoma de Madrid
[33] Mott N F 1974 *Metal–Insulator Transitions* (London: Taylor and Francis)
[34] Hwang H Y and Cheong S-W 1997 *Nature* **389** 942
[35] Zallen R A 1983 *The Physics of Amorphous Solids* (New York: Wiley)
[36] Helman J S and Abeles B 1976 *Phys. Rev. Lett.* **37** 1429
[37] Ziese M 2002 *Appl. Phys. Lett.* **80** 2144